Determining the three-phase coexistence line in methane hydrates using computer simulations

M. M. Conde and C. Vega[a)]
Dept. Química-Física I, Facultad de Ciencias Químicas, Universidad Complutense de Madrid, 28040 Madrid, Spain

(Received 12 March 2010; accepted 29 June 2010; published online 12 August 2010)

Molecular dynamics simulations have been performed to estimate the three-phase (solid hydrate-liquid water-gaseous methane) coexistence line for the water-methane binary mixture. The temperature at which the three phases are in equilibrium was determined for three different pressures, namely, 40, 100, and 400 bar by using direct coexistence simulations. In the simulations water was described by using either TIP4P, TIP4P/2005, or TIP4P/Ice models and methane was described as simple Lennard-Jones interaction site. Lorentz–Berthelot combining rules were used to obtain the parameters of the cross interactions. For the TIP4P/2005 model positive deviations from the energetic Lorentz–Berthelot rule were also considered to indirectly account for the polarization of methane when introduced in liquid water. To locate the three-phase coexistence point, two different global compositions were used, which yielded (to within statistical uncertainty) the same predictions for the three-phase coexistence temperatures, although with a somewhat different time evolution. The three-phase coexistence temperatures obtained at different pressures when using the TIP4P/Ice model of water were in agreement with the experimental results. The main reason for this is that the TIP4P/Ice model reproduces the melting point of ice I_h. © *2010 American Institute of Physics*. [doi:10.1063/1.3466751]

I. INTRODUCTION

Gas hydrates are crystalline, nonstoichiometric inclusion compounds[1] formed under high pressure and at moderately low temperatures. Their structure consists of a three-dimensional framework of hydrogen-bonded water molecules within which are incorporated a small number of relatively inert "guest" molecules, such as CH_4, C_2H_6, C_3H_8, iC_4H_{10}, CO_2, and H_2S. Also N_2, O_2, H_2, noble gases, and hydrocarbons such as cyclopropane can form hydrates. Most hydrates are classified into three crystalline structures sI (Ref. 2) (cubic structure), sII (Ref. 3) (cubic structure), and sH (Ref. 4) (hexagonal structure) according to the arrangement of the water molecules, which is determined mainly by the size of the guest molecules. The molecules occupying the cavities of the host lattice should be neither too large nor too small to yield a stable hydrate.[1,5,6] Thus, it is not possible to study empty hydrates using experimental methods since they are thermodynamically unstable, although they can be studied by computer simulation[7–14] due to their mechanical stability. In our earlier work, we performed computer simulation studies using empty hydrates to estimate the phase diagram of water at negative pressures[8] and the difference in the chemical potential between ice I_h and the empty hydrates, which plays a central role within the widely used van der Waals–Platteeuw theory.[15] It was found that the empty hydrate structures sII and sH become thermodynamically stable at negative pressures.[8] This is in agreement with the results of Molinero *et al.*[9] who, using a coarse grained model of water, also found the sII structure to be stable at negative pressures. Moreover, we have studied the quantum nuclear effects on empty hydrates analyzing several properties such as energy, density, the radial distribution function, and the heat capacity.[14]

Since their discovery,[16] a large number of gas hydrate systems have been studied[6,17–23] for their scientific interest as well as the role they play in industry and the environment. Recently, the sII and sH hydrates have attracted great interest[24–29] due to the possibility of being used for hydrogen storage. Also, it has been proposed that oceans can store carbon dioxide in the hydrate form to mitigate its greenhouse effect.[30–33] In the area of medicine hydrate structures have been suggested as a medium for organ preservation.[34]

In nature[1,35,36] there are vast quantities of methane hydrate on the deep ocean regions where the presence of pressure combined with low temperatures favors its formation[31,37,38] providing a potential fuel reserve beyond conventional fossil fuel deposits.[39] The use of methane hydrates found on the sea floor as an energy source has attracted considerable interest in many countries. However, if released, the methane trapped in hydrate form in large amounts in oceans[40] will contribute significantly to global warming. On the other hand, the formation of these compounds can cause problems in the flow of gas in natural gas pipelines, additives being needed that act as inhibitors.[1,41–45]

Therefore, it is desirable to predict the conditions under which one should expect that these compounds are formed. In recent times, computer simulation has become a useful tool to draw qualitative conclusions when applied to real systems.[46–61] A significant number of simulations have been performed for the methane hydrates[62–83] that have helped us

[a)]Electronic mail: cvega@quim.ucm.es.

TABLE I. Number of molecules situated in the different phases for two systems A and B studied in this work. Methane mole fraction is denoted by x_{CH_4}. We have also studied a system with double size of that of system A and we have denoted it as system A'.

System	Hydrate phase	Liquid phase	Vapor phase	Mole fraction (x_{CH_4})
A	368 water/64 methane	368 water	64 methane	~0.15
A'	736 water/128 methane	736 water	128 methane	~0.15
B	368 water/64 methane	368 water	128 methane	~0.21

to understand the behavior of these compounds from a molecular point of view. However, there are still many questions that are unresolved in the simulation of methane hydrates, for instance, the mechanism of nucleation and growth. Recently, a study has been published by computer simulation of spontaneous methane hydrate nucleation and growth[84,85] using the TIP4P/Ice model proposed by Abascal *et al.*[86] for water along with a simple Lennard-Jones interaction for methane. The Lennard-Jones parameters used in that work were taken from Ref. 87. In this study a possible mechanism for the nucleation and growth of hydrates has been proposed which is in line with previous suggestions.[74,75,88,89] It should be pointed out that at this moment the three-phase coexistence line (hydrate-water-methane) and the four phase coexistence point (ice-hydrate-water-methane) for most of the models considered in simulation studies are still unknown. One exception is the studies of Wierzchowski and Monson[90,91] who determined coexistence lines using a primitive model[92,93] of water and a simple model of methane. According to the Gibbs phase rule, for a binary system there is only one degree of freedom when three phases are present (forming lines on the $p-T$ projection of the phase diagram) and zero degrees of freedom when four phases are present (yielding a singular quadruple point on the $p-T$ projection of the phase diagram). Experimentally, the three-phase coexistence line and the quadruple point of the binary water-methane mixture are well known.[1] The aspect of the phase diagram obtained by Wierzchowski and Monson was in agreement with the experimental one. Also Westacott and Rodger determined the pressure (at a certain temperature) at which the methane hydrate becomes unstable with respect to ice Ih and methane.[94]

Thus, there is an increasing interest in studying methane hydrates by computer simulation. These studies are needed to achieve good understanding of the molecular mechanism of nucleation and growth for these compounds. The main goal of this paper is to estimate the three-phase (hydrate-water-methane) coexistence line using different potential models of water. A comparison with experimental results will illustrate the limitations of the models, and also will show which, if any, among the several water models used in this work (TIP4P,[95] TIP4P/2005,[96] TIP4P/Ice[86]) reproduces the experimental results. From a technical point of view this paper will show that direct coexistence simulations,[97–99] which were used successfully to find melting points[100] of water models, can also be used for binary mixtures to search for three-phase coexistence conditions.

II. METHODOLOGY

Methane hydrate adopts the sI structure. It is simple cubic and has the space group $Pm\bar{3}n$. The unit cell contains eight water cages (six tetradecahedra $5^{12}6^2$ and two dodecahedra 5^{12}). The unit cell consists of 46 H_2O and eight CH_4 molecules. For our study we used a methane hydrate configuration of $2\times2\times2$ unit cells (a total of 368 water molecules and 64 methane molecules). The crystallographic parameters of the methane hydrate were taken from Yousuf *et al.*[101]

To generate the initial configuration we followed the methodology proposed by Fernandez *et al.*[100] obtaining a system formed by a slab of liquid water surrounded at one side by a slab of the methane hydrate and at the other site by a slab of methane molecules in the gas phase. In system A, the slab containing the methane molecules in the gas phase contains 64 molecules. In system B, the slab containing the methane molecules in the gas phase contains 128 molecules. The global (including all phases within the simulation box) mole fraction of methane in system A is $x_{CH_4}\sim0.15$, whereas its value for system B is $x_{CH_4}\sim0.21$. The details about the composition of the phases are given in Table I. The typical size of the simulation box for the initial configuration was $55\times24\times24$ Å^3 (system A) and $67\times24\times24$ Å^3 (system B). The interfaces between the three phases are perpendicular to the x axis. From 67 Å in the direction perpendicular to the interface, about 24 Å was occupied by methane hydrate, about 22 Å by water, and about 21 Å by methane gas. Hydrates present proton disorder.[102–104] We used the algorithm proposed by Buch *et al.*[105] to generate solid configurations satisfying the Bernal–Fowler rules[106] and with zero (or almost zero) dipole moment for the sI hydrate. Periodic boundary conditions were employed in the three directions of space. The initial arrangements permit us to have each phase in contact with the other two. The number of methane molecules with the same value of x (the direction perpendicular to the fluid/solid interface) in our seed crystal (which contains $2\times2\times2$ unit cells of the sI hydrate) is 12, 4, 12, 4, 12, 4, 12, 4 (i.e., 64 methane molecules in total). Layers containing 12 methane molecules are formed by the large cavities, whereas layers formed by four methane molecules correspond to the small cavities. Since our seed crystal acts as a template for the growth of the hydrate, each new layer during the hydrate growth contains either 12 or 4 methane molecules.

Figure 1 shows the experimental temperature-composition coexistence diagram of the methane-water mixture for a certain fixed pressure as reproduced artistically

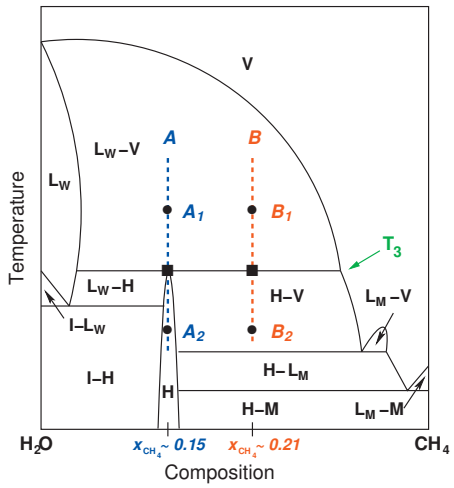

FIG. 1. Experimental CH_4–H_2O T-x phase diagram in the range $p \approx 500$ bar [artistically reproduced from Huo *et al.*(Ref. 107)]. V: Vapor. L_W: Liquid water. H: Hydrate. M: Solid methane. L_M: Liquid methane. I: Ice. (■) corresponds to the initial configuration of systems A (water +hydrate+64 methane molecules) and B (water+hydrate+128 methane molecules) with a methane mole fraction of 0.15 and 0.21, respectively. A_1, A_2, B_1, and B_2 are equilibrium states (●). The temperature where the three phases coexist is defined by the T_3 line. Region expanded for better display.

from Ref. 107. In Fig. 1 the two compositions considered in this work are represented by vertical lines. The global molar fraction of methane in system A is exactly the same as that of the pure methane hydrate (the molar fraction of methane in the pure hydrate can be obtained easily taking into account that the unit cell of the sI solid has 46 water and eight methane molecules). The global molar fraction of methane in system B is slightly higher than that of the pure hydrate. As can be seen in Fig. 1, the temperature at which the three phases coexist (methane hydrate H, liquid water L_W, and methane vapor V) is denoted as T_3. Starting from an initial configuration formed by a slab of methane hydrate, a slab of liquid water, and another of methane vapor with either $x_{CH_4} \sim 0.15$ (system A) or $x_{CH_4} \sim 0.21$ (system B) global mole fractions of methane the system will evolve to an equilibrium state A_1 or B_1 when the temperature is above T_3 or states A_2 or B_2 when the temperature is below T_3. In states A_1 and B_1 two phases, liquid water and methane, are in equilibrium (with small amounts of the other component in each phase). In state A_2 there is only one phase (i.e., the pure methane hydrate). In state B_2 there are two phases, the methane hydrate and the methane gas. Notice that if by chance one performs simulations at exactly the coexistence temperature T_3 then the three phases of the initial configuration will remain in equilibrium, both for system A and for system B. Obviously the probability of selecting T_3 exactly (with all significant figures) is zero so that in practice the system (for a certain fixed pressure) will evolve either to states with subscript 1 (when the temperature is above T_3) or to states with subscript 2 (when the temperature is below T_3).

We performed NpT molecular dynamic simulations at different temperatures and pressures at 40, 100, and 400 bar using the molecular dynamics package GROMACS (version 3.3).[108] The temperature was fixed using a Nosé–Hoover thermostat[109,110] with a relaxation time of 2 ps. To keep the pressure constant, a Parrinello–Rahman barostat[111,112] was used. The relaxation time of the barostat was 2 ps. The three different sides of the simulation box were allowed to fluctuate independently to allow changes in the shape of the solid region and to avoid the existence of stress in the solid. The time-step used in the simulations was 2 fs. The typical length of the simulations depended on the conditions of pressure and temperature. At 400 bar the average length was 50 ns and at 40 bar about 300 ns. These differences will be discussed later. The geometry of the water molecules was enforced using constraints.[113,114] The Lennard-Jones part of the potential was truncated at 9 Å. Ewald sums were used to deal with electrostatics. The real part of the Coulombic potential was truncated at 9 Å. The Fourier part of the Ewald sums was evaluated by using the particle mesh Ewald method of Essmann *et al.*[115] The width of the mesh was 1 Å and we used a fourth order polynomial.

Although methane is a nonspherical molecule, it may be described reasonably well by using a spherical Lennard-Jones (LJ) interaction site. In our simulations we used the parameters proposed by Guillot and Guissani[116] and Paschek.[117] TraPPE (Ref. 118) and OPLS-UA (Ref. 119) are other popular models for methane. These models are similar to the model used here. The value of σ is the same. The difference lies in the value of ϵ/k_B, being about 148 K instead of 147.5 K as used in this work. TIP4P,[95] TIP4P/2005,[96] and TIP4P/Ice[86] models were used for water-water interactions. These water models are rigid and nonpolarizable. For all these water models, a LJ interaction site is located on the oxygen atom, positive charges are located on the positions of the H atoms, and the negative charge is located at a distance d_{OM} from the oxygen along the H–O–H bisector. The potential parameters for these models are given in Table II.

The water-methane interaction is often described using a LJ potential with the cross interaction parameters given by the Lorentz–Berthelot rules. Docherty *et al.*[120] developed a model able to describe correctly the excess chemical potential of methane in water over a wide range of temperature. They observed that the experimental values of the chemical potential were not reproduced when using the Lorentz–Berthelot combining rules. The deviation was systematic. Introducing positive deviations from the energetic Lorentz–Berthelot rule to indirectly account for the polarization methane-water energy, they were able to accurately describe the excess chemical potential of methane in water. The combination rule used in this work for the LJ parameters of the water-methane interaction is given by

$$\epsilon_{CH_4\text{–}H_2O} = \chi \sqrt{\epsilon_{CH_4\text{–}CH_4} \cdot \epsilon_{H_2O\text{–}H_2O}}, \tag{1}$$

$$\sigma_{CH_4\text{–}H_2O} = \frac{(\sigma_{CH_4\text{–}CH_4} + \sigma_{H_2O\text{–}H_2O})}{2}. \tag{2}$$

When $\chi = 1$ the Lorentz–Berthelot combining rules[121] are recovered. However, deviations from the Lorentz–Berthelot rule are obtained when $\chi \neq 1$.

Docherty *et al.*[120] used the TIP4P/2005 model for water and increased the cross interaction energy from that obtained

TABLE II. Potential parameters of the TIP4P (Ref. 95), TIP4P/2005 (Ref. 96), and TIP4P/Ice (Ref. 86) models. The distance between the oxygen and the hydrogen sites is d_{OH}. The angle, in degrees, formed by hydrogen, oxygen, and the other hydrogen atom is denoted by ∠H–O–H. The Lennard-Jones site is located on the oxygen with parameters σ and ϵ. The charge on the proton is q_H. The negative charge is placed on a point M at a distance d_{OM} from the oxygen along the H–O–H bisector. The LJ interaction parameters for methane are taken from Refs. 116 and 117.

Model	d_{OH} (Å)	∠H–O–H	σ (Å)	ϵ/k_B (K)	q_H (e)	d_{OM} (Å)
TIP4P	0.9572	104.52	3.1540	78.02	0.52	0.15
TIP4P/2005	0.9572	104.52	3.1589	93.2	0.5564	0.1546
TIP4P/Ice	0.9572	104.52	3.1668	106.1	0.5897	0.1577
CH_4			3.730	147.5		

from Lorentz–Berthelot [by using $\chi=1.07$ in Eq. (1)] as an effective way of accounting for the polarization of methane when dissolved in water. They applied this methane-water potential to the study of the solid methane hydrate structure and found that the model described the experimental value of the unit cell of the hydrate with an error of about 0.2%. The impact of using a polarizable solute model with rigid water models has been studied by Dyer *et al.*[122] Also, alternative combining rules, such as the Kong combining rules,[123] have been used to predict the phase equilibrium for mixtures of polar and nonpolar components[124] and for water-*n*-butane and water-*n*-hexane systems.[125] Table III shows the cross interaction for the different models used in this study. Notice that the value of $\epsilon_{CH_4-H_2O}$ obtained using the TIP4P/Ice model of water with $\chi=1$ is almost identical to that obtained using the TIP4P/2005 model with $\chi=1.07$ so that the strength of the water-methane interactions is similar in both models.

In our study the configuration of hydrate has 100% of the cages occupied by methane. From a dynamic point of view English *et al.*[126] and Myshakin *et al.*[81] found that the decomposition rate does not depend strongly on the cage occupancy over 80%–100% occupancy. From a thermodynamic point of view it is expected that the occupation of the methane in the hydrate at equilibrium (i.e., when the solid presents the lowest possible free energy) is quite high but certainly not 100%. Although it is expected that the lower occupation of methane will move somewhat the three-phase coexistence line (to higher temperatures), it is expected that the effect will be quite small. In any case, this issue could be analyzed in more detail in future studies. English and Phelan[127] also reported a study of methane hydrate dissociation where the value of the melting point for the 85% and 95% occupied systems was found to be similar to the fully occupied case.

TABLE III. Cross interaction parameters for the water-methane interaction as obtained from Lorentz–Berthelot rules ($\chi=1$) and from the optimized potential ($\chi=1.07$) taken from the work of Docherty *et al.*(Ref. 120).

Cross interaction	χ	ϵ/k_B (K)	σ (Å)
TIP4P-CH_4	1	107.28	3.442
TIP4P/Ice-CH_4	1	125.10	3.4484
TIP4P/2005-CH_4	1	117.25	3.4445
TIP4P/2005-CH_4	1.07	125.45	3.4445

Let us now present some numbers about the order of magnitude of several properties that are relevant for the present study. Results will be discussed for the TIP4P/2005. As to the diffusion coefficient of methane in water we found 1.33×10^{-9} and 0.46×10^{-9} m^2/s for 300 and 265 K, respectively, at 400 bar. The diffusion coefficient did not change much with the applied pressure. The solubility of methane in TIP4P/2005 water at 373 K has been determined by computer simulation by Biscay *et al.*[128] To estimate the solubility we have determined Henry's constant at 280 K for methane in TIP4P/2005 water (with a value of $\chi=1$) finding it to be 4.24×10^4 bar. From this value the molar fraction of methane in the liquid phase was estimated to be about 9.31×10^{-4}, 2.35×10^{-3}, and 9.43×10^{-3} for 40, 100, and 400 bar, respectively. Taking into account that the liquid phase has 368 molecules, the number of methane molecules in the water phase is about 0.34, 0.86, and 3.47 for the pressures of 40, 100, and 400, respectively. The surface tension at 300 K of the vapor-liquid interface of pure water when using TIP4P/2005 (Refs. 129 and 130) is 69 mJ/m^2. It is expected that the surface tension for the water-methane interface will be about 3 mJ/m^2 lower (at 40 bar) and about 12 mJ/m^2 lower at 400 bar (that was the reduction found by Biscay *et al.*[128] for this model at 373 K). Notice that for systems of this side the surface contribution to the total free energy between fluid phases may be quite important and may be responsible for driving the fluid phases into a single phase. This is especially true for system *A* where the number of methane molecules in the gas phase is rather small (64).

III. RESULTS

The energy is expected to fluctuate in *NpT* simulations. Systematic changes in the energy should only be associated with phase transitions. For system *A*, at high temperatures the region formed by hydrate will melt, resulting in a system with two phases (liquid water and methane) when reaching the equilibrium state denoted as A_1. However, at low temperatures the water and methane will freeze forming a unique phase of hydrate when reaching the equilibrium state denoted as A_2. At a certain temperature the three phases will be

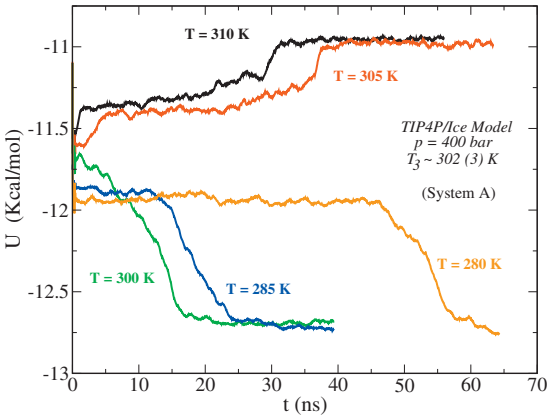

FIG. 2. Evolution of the potential energy as a function of time for the *NpT* runs for TIP4P/Ice at 400 bar for three-phase system *A* (water+hydrate +64 methane molecules). The values are the rolling averages. Results for only a few representative temperatures are shown.

in equilibrium. We will denote this temperature (i.e., the three-phase coexistence temperature for a considered pressure) as T_3.

We shall start by presenting the results obtained for the TIP4P/Ice model of water. The time evolution of the potential energy as a function of time for the system with global composition *A* at a fixed pressure of 400 bar is shown in Fig. 2. In the initial configuration we have a three-phase system composed by methane hydrate, liquid water, and vapor phase. For all temperatures we used the same initial configuration. As can be seen in Fig. 2, the initial energy of the system at different temperatures is slightly different. This is due to the fact that the system relaxes very quickly (in about 0.1 ns) from the initial configuration (where the energy is the same regardless of the temperature) to a relaxed one, and this short time cannot be visualized properly on the long time scale selected when plotting Fig. 2. To facilitate the visual presentation we have displayed the rolling averages of the total energy and only the most representative temperatures have been plotted. Remember that in our *NpT* Molecular Dynamics (MD) runs, we allow each side length to fluctuate independently. This is important since it allows to accommodate the molecules of the melted hydrate in the fluid phase (or conversely to accommodate into the solid structure the molecules that are freezing). For temperatures above T_3 the potential energy increases with time, indicating the melting of the solid phase (i.e., the methane hydrate). This is the case for the temperatures of 305 and 310 K, which are plotted in Fig. 2. The plateau that is visible for these two temperatures at long simulation times corresponds to an equilibrium state of type A_1 (see the meaning of A_1 in the sketch presented in Fig. 1). Although the melting of the hydrate is a stochastic process (to obtain definitive conclusions the average of many independent runs should be analyzed) it seems that the hydrate melts sooner as the temperature is increased. The same behavior was found in direct coexistence simulations of pure water when simulating the ice I_h-water two phase system. From the inspection of the results of Fig. 2 we can infer that for temperatures above T_3, the complete melting of the methane hydrate causes an overall increase of the potential energy of about 0.7 kcal/mol.

Let us now present the curves for temperatures below T_3. Results are presented in Fig. 2 for the temperatures of 300, 285, and 280 K. For temperatures below T_3 one should expect the growth of the methane hydrate being the mass transport the limiting factor determining the growth rate (heat transport could also be important in real experiments, but here it does not play such a relevant role since the thermostat takes/provides energy from the system very quickly). As such, it is obvious that transport of methane to the hydrate/water interface must occur before growth can take place. Since the vapor pressure of water is so low under these conditions, growth of the methane hydrate from the gas/methane hydrate interface does not occur.

For the temperature of 300 K the energy decreases from the very outset and complete freezing is obtained in about 20 ns. For a temperature of 285 K the energy decreases slowly in the first 15 ns and then decreases suddenly until the system freezes completely in the subsequent 15 ns. For the temperature of 280 K the energy decreases very slowly in the first 45 ns and then decreases quickly reaching complete freezing after 15 ns. The final plateau in the energy for runs with temperature below T_3 indicates the complete crystallization of the fluid phases with complete formation of the methane hydrate. The complete freezing of the fluid (liquid water and gas methane) is reflected by an overall decrease in the potential energy of about 0.7 kcal/mol. The fast growth of the methane hydrate (manifested by a significant drop in the potential energy) occurs once a supersaturated solution of methane in water is formed. The supersaturated solution is generated when the bubble (containing all the molecules of methane of the gas phase) is broken. The bubble that we observe is not spherical. It is rather a cylindrical bubble in agreement with that observed by Jacobson and Molinero[131] in their recent study of the methane-water mixture using a coarse grained model of the mixture. MacDowell *et al.*[132] discussed the conditions for the formation of spherical, cylindrical, and slablike droplets and bubbles when simulating small system with simple potential models. The sequence of events is disappearance of the planar gas/water interface after the formation of a methane cylindrical bubble, formation of a supersaturated methane in water solution once the bubble is broken, and fast growth of the methane hydrate from the supersaturated solution. The formation of methane bubbles in computer simulations has been reported previously by Vatamanu and Kusalik[133,134] and Walsh *et al.*[84] In Fig. 3 the formation of the cylindrical bubble for system *A* (with water described by the TIP4P/Ice model) at 400 bar and 285 K is clearly seen. The cylindrical bubble is stable only for a few nanoseconds, and after that time all the methane within the bubble is dissolved into the liquid water creating a supersaturated solution of methane in water. Since the water solution now contains large amounts of methane, the growth of the methane occurs rather quickly (i.e., in about 15 ns). Once the gas phase has disappeared methane growth occurs in two hydrate/water solution interfaces. In summary the growth rate of the methane hydrate is slow when the water film separates the methane hydrate from the gas and occurs quickly once a supersaturated solution of methane in water is formed soon after the formation of the cylindrical bubble. It

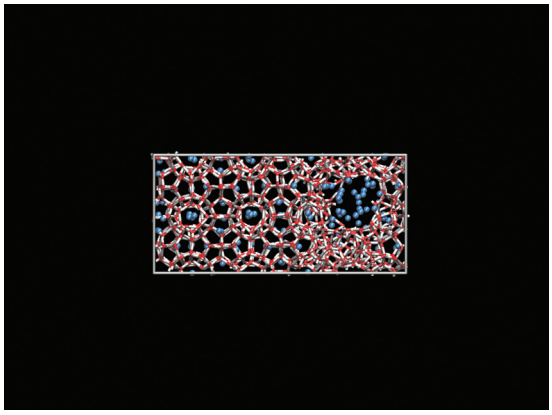

FIG. 3. Snapshot of TIP4P/Ice model for the system A at 400 bar and 285 K taken at the instant at which a cylindrical bubble of methane in water forms.

should be pointed out that bubble formation should be incredibly rare under marine conditions[135] and that system size effects are enhancing the ease of bubble formation in the present study. In fact we have performed a run at 400 bar and 290 K for the TIP4P/Ice model using a system with the same composition than that of system A but with twice as many molecules (keeping the area of the interface and multiplying the length along the x axis by a factor of 2). We denoted this system as system A'. Details are given in Table I. Simulations of this system are quite expensive from a computational point of view. After running 700 ns we observed a continuous decrease of the energy without observing bubble formation, thus confirming that finite size effects are important when considering bubble formation. Nevertheless, also for system A' the formation of bubble at the end of the growth process is expected (although extremely long runs would be required to obtain total crystallization of the mixture for this system size). The evolution of the potential energy as a function of time for system A' is given by Fig. 4.

Let us now discuss the similarities and differences between the time evolution of the potential energy for temperatures below T_3 and that found in direct coexistence simulations of the I_h-water system at temperatures below the melting point. For the I_h-water interface runs at temperatures

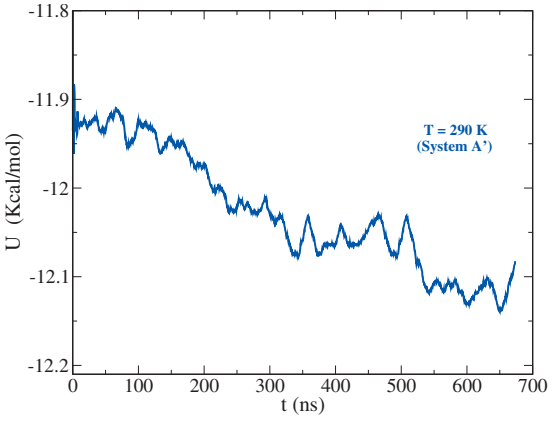

FIG. 4. Evolution of the potential energy as a function of time for the NpT runs for TIP4P/Ice at 290 K and 400 bar for three-phase system A' (system with the same composition than system A but with twice as many molecules). Rolling average is used for the value of the potential energy.

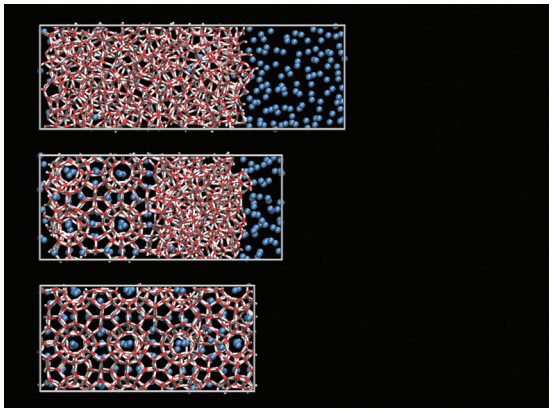

FIG. 5. Snapshots of TIP4P/Ice model for system A containing water, methane hydrate, and 64 methane molecules with a total of 864 molecules at 400 bar. The initial configuration is shown in the middle, whereas the final configuration at 310 K state A_1 is shown on the top and the final configuration at 285 K state A_2 is shown at the bottom.

below the melting point, the energy continuously decreases from the very beginning causing the steady growth of the ice phase, which is completed typically after 15 ns. Here in the case of the methane hydrate, the energy decreases very slowly with time while the water film separates the hydrate from the gas (mass transport controlling the growth rate), but can be accelerated considerably if the methane hydrate is brought into contact with a supersaturated solution of methane in water. In summary one may expect reasonable rates for the growth of solids when the molecules forming the solid are available at the solid-fluid interface.

The thermodynamic consequence of the results presented in Fig. 2 is that the methane hydrate melts for temperatures above 305 K, and the system freezes completely for temperatures below 300 K. We will estimate T_3 as the arithmetic average of the lowest temperature at which the methane hydrate melts and the highest temperature at which the system freezes. According to this criterion, the three-phase coexistence temperature for the TIP4P/Ice model of water and the LJ model of methane is $T_3=302(3)$ K at 400 bar. This is in good agreement with the experimental value at this pressure which is 297 K.[1] The good agreement is certainly satisfying and the reader may be somewhat surprised; the experimental three-phase coexistence line of the methane hydrate starts at a temperature very close to the melting point of ice I_h. Thus, having a water model able to reproduce the experimental melting point of ice helps significantly in describing the experimental three-phase coexistence points. Snapshots of the final configurations obtained for system A at 400 bar at two temperatures are presented in Fig. 5. In the central panel of Fig. 5 the initial configuration of the runs is presented. The final configuration for state A_1 (310 K) is presented in the upper panel, whereas in the lower panel the final configuration of state A_2 (285 K) is shown. Obviously at 310 K the methane hydrate has melted completely, whereas at 285 K the fluid phases have frozen increasing the size of the initial methane hydrate slab. It should be pointed out that the methane occupancy obtained at the end of the run of state A_2 (285 K) is 100%. In a real system of this composition, at perfect equilibrium the system would

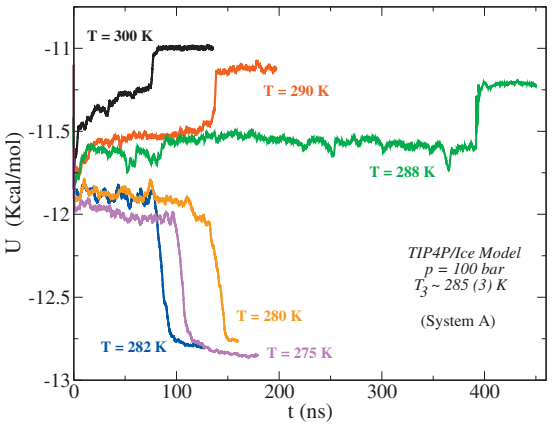

FIG. 6. Evolution of the potential energy as a function of time for the *NpT* runs for TIP4P/Ice at 100 bar for the three-phase system *A* (water +hydrate+64 methane molecules). The values are the rolling averages. Results for only a few representative temperatures are shown.

still have two phases present: gas and hydrate (with an occupancy lower than 100%). But in a system the size of this simulation, surface tension probably drives a higher cage occupancy to avoid the presence of any interface. It would be interesting to analyze this in more detail in future studies.

Some aspects that may affect the value of the coexistence temperature are the initial solid configuration (sI hydrate presents proton disorder, thus there is no unique initial solid configuration) and finite size effects. We found in previous work that the free energy differences between different proton disordered configurations are small for crystals having more than 300 water molecules. For this reason we do not expect big changes in the value of T_3 when using different proton disordered configurations for the initial methane hydrate slab. Also for pure water we have found[100] that system size effects in direct coexistence simulations are small, at least for system having about 1000 particles, which is roughly the size of the system considered here.

In Figs. 6 and 7 the results of several *NpT* runs for the TIP4P/Ice model at 100 and 40 bar are presented. To aid visualization in Figs. 2, 6, and 7 the results are presented for selected temperatures. The trend of the curves is similar to those found at 400 bar. The main difference is that as the pressure decreases longer runs are required to either completely melt the hydrate or to completely freeze the fluid phase. For 400 bar, runs of about 50 ns were sufficient. At 100 bar, runs of about 400 ns were required, and finally for 40 bar it was required to go to runs of about 800 ns. In general, melting occurs sooner as the temperature increases. For the runs at 100 bar the time required to freeze the system seems to be independent of the temperature. Typically after an induction time of about 100 ns (i.e., the time required for the formation of the bubble) freezing occurs in about 15 ns. At the lowest pressure the time needed by the system to form the cylindrical bubble (i.e., the induction time) increases as the temperature increases. Thus, the results can be summarized by saying that melting occurs sooner as the temperature increases (except at 40 bar). At 40 bar that difference may be due to stochastic nature of the runs. Freezing occurs within similar times regardless of the temperature for the intermediate pressure, $p=100$ bar. At low pressures freezing requires more time as the temperature increases, whereas at high pressures freezing requires more time as the temperature decreases. Although these kinetic aspects are interesting, the important point here is that the coexistence lines allow us to estimate the value of T_3 for the three pressures considered in this work. Also, in some of our trajectories for the study of growth in system *A*, we observed the presence of a few defects[136] in the crystals, apparently independent of the imposed conditions of pressure and temperature and the potential model used.

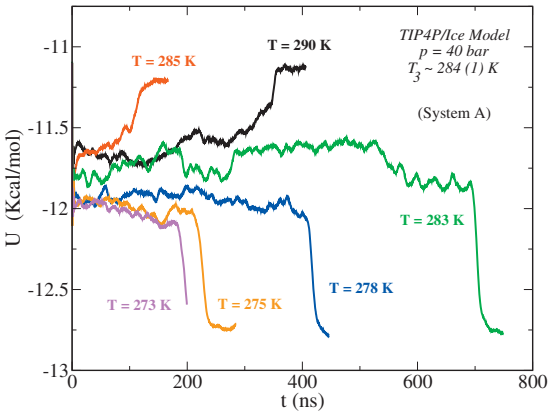

FIG. 7. Evolution of the potential energy as a function of time for the *NpT* runs for TIP4P/Ice at 40 bar for the three-phase system *A* (water+hydrate +64 methane molecules). The values are the rolling averages. Results for only a few representative temperatures are shown.

Let us now present the results for system *B* which has an overall higher mole fraction of methane than system *A*. The motivation to study system *B* is twofold. First, the estimate of T_3 obtained by performing simulations of system *B* should be identical (within the statistical uncertainty) to that obtained for system *A* and that will constitute a cross-check of the methodology used in this work. The reason why T_3 should be independent on composition can be seen more clearly in the sketch of Fig. 1, where it is obvious that the temperature at which the three phases are in equilibrium should be identical for the system with compositions *A* or *B*. Direct coexistence simulations were then performed for a system with composition *B*. Analyzing the trajectories we observed that at high temperatures the methane hydrate melts and the final equilibrium configuration corresponds to that of a two phase system (liquid water and methane). At low temperatures we observed growth of the methane hydrate and in the final equilibrium configuration two phases can be found, methane hydrate and methane gas. Figure 8 shows snapshots of the initial configuration and of the final ones for the TIP4P/Ice model at two different temperatures at 400 bar for system *B*. The final configuration at 285 K (bottom) corresponds to two phases in coexistence (hydrate and methane). At 310 K (top) the equilibrium state B_1 is shown. Our estimate of T_3 for system *B* is 297(8) K, which agrees to within statistical uncertainty with the value obtained for system *A*, 302(3) K. Thus the methodology can also be applied for the system with composition *B*. For system *B* we performed only a few simulations since it has a higher computational cost (see the discussion below), and for this reason the uncer-

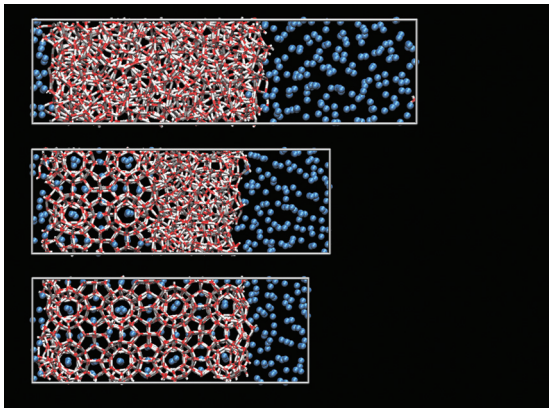

FIG. 8. Snapshots of TIP4P/Ice model for the system *B* containing water, methane hydrate, and 128 methane molecules with a total of 928 molecules at 400 bar. The initial configuration is shown in the middle. The final configuration at 310 K state B_1 is shown in the upper panel, whereas the final configuration at 285 K state B_2 is shown in the lower panel.

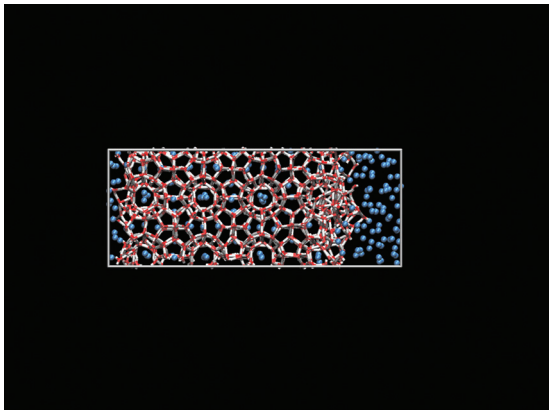

FIG. 10. Snapshot of TIP4P/Ice model for system *B* at 400 bar and 285 K at time of growth of the last layer of hydrate. The figure shows the formation of this layer through the interface and not a mechanism for bubble formation.

tainty of our estimate of T_3 from runs of system *B* is higher than that of system *A*. In the melting process, the decomposition rate for both systems (A and B) is about 0.7 Å of hydrate/ns. This is shown in Fig. 9. This rate is similar to that found by Myshakin *et al.*[81] for the COS/G2 model[137] of water when simulated at 10 K above the value of T_3 for their model. Let us now focus on the freezing rate for systems *A* and *B*. This is shown again in Fig. 9. In system *A* freezing occurs by the formation of a cylindrical bubble (see Fig. 3) and soon after of a supersaturated solution of methane in water. For the conditions shown here, a system of type *A* at 10 K below T_3, it took about 15 ns (after the formation of the cylindrical bubble) to grow the methane solid by about 24 Å. Once the supersaturated methane solution is formed there are two hydrate surfaces to template growth. Growth is observed in both interfaces, and for this reason the estimated growth rate is about 0.8 Å/ns. In system *B* the formation of the bubble is not observed. Rather the energy continuously decreases along the run. Inspection of the freezing trajectories of system *B* reveals that the methane hydrate grows very slowly layer by layer. This is further illustrated in Fig. 10 where a snapshot of system *B* just before the crystallization of the last hydrate layer is shown. For system *B* the small amount of methane in water (due to its low solubility) is controlling the growth rate. For system *B* it takes about 700 ns to grow 24 Å of hydrate so that the growth rate is about 0.03 Å/ns. Comparison of these numbers with experimental growth rates is somewhat risky. In the real system growth is usually limited by methane diffusion, and this will depend on the thickness of the water film separating the methane source from the hydrate surface.

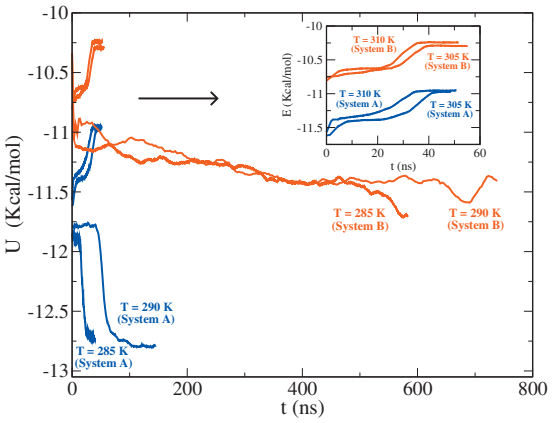

FIG. 9. Evolution of the potential energy as a function of time along the *NpT* runs for TIP4P/Ice at 400 bar and at different temperatures for systems *A* and *B*. The figure shows the same behavior in the melting process (top) and different behavior in the process of growth of methane hydrate (bottom). For a better visualization of the figure the melting process (top) has been shown in the inset.

In Table IV the values of T_3 obtained for the TIP4P/Ice model at the three considered pressures are presented. Ex-

TABLE IV. Three-phase coexistence temperatures (T_3) at different pressures for different water models as obtained from simulations of systems of type *A* and/or *B*. The estimated error in T_3 is shown within the parentheses. The experimental values are taken from Ref. 1. The melting temperature of ice I_h is given by T_{m,I_h} and its value for the different models is taken from Refs. 100 and 138.

Model	p (bar)	System	T_3 (K)	T_3-T_{m,I_h} (K)
TIP4P	400	*A*	256 (2)	26
T_{m,I_h}=230 K	400	*B*	252 (8)	22
	100	*A*	247 (3)	17
	40	*A*	244 (4)	14
TIP4P/2005 (χ=1)	400	*A*	276 (2)	26
T_{m,I_h}=250 K	400	*B*	272 (7)	22
	100	*A*	265 (3)	15
	100	*B*	265 (15)	15
	40	*A*	263 (3)	13
TIP4P/2005 (χ=1.07)	400	*A*	281 (2)	31
T_{m,I_h}=250 K	100	*A*	274 (4)	24
	40	*A*	267 (3)	17
TIP4P/Ice	400	*A*	302 (3)	32
T_{m,I_h}=270 K	400	*B*	297 (8)	27
	100	*A*	285 (3)	15
	40	*A*	282 (4)	12
Experimental	400	···	297	~24
T_{m,I_h}=273.15 K	100	···	286	~13
	40	···	278	~5

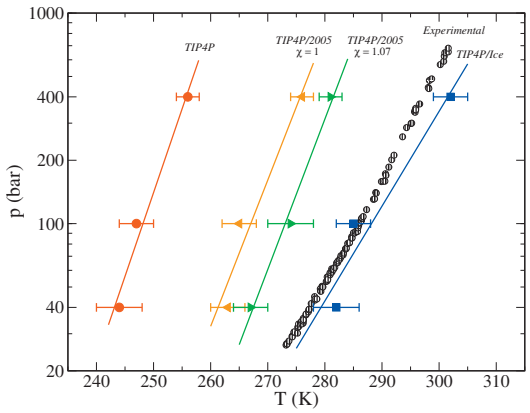

FIG. 11. Representation of the three-phase (water-hydrate-methane) coexistence temperature T_3 as a function of pressure for several potential models. Experimental results were taken from Ref. 1. For each model the lines correspond to a fit of the simulation results.

perimental values are also reported. As can be seen the values of T_3 obtained for the TIP4P/Ice model are in reasonable agreement with the experimental ones. We have repeated the methodology described for the TIP4P/Ice with other water models (while maintaining the same potential). The aspects of the plots, the kinetics mechanism, and the rest of the details were similar to those already presented for the TIP4P/Ice. In Table IV the values of T_3 for TIP4P, TIP4P/2005, and TIP4P/2005 models (with positive deviations from the energetic Lorentz–Berthelot rule) are presented. Most of the results presented in Table IV were obtained using system *A*. However, in a few cases T_3 was also determined using system *B*. Since simulations of system *B* are computationally more expensive only a few temperatures were studied. As it can be seen the results of T_3 for systems *A* and *B* agree within statistical uncertainty. It can be seen that the TIP4P and TIP4P/2005 models underestimate the experimental values of T_3 for all pressures. This is more clearly seen in Fig. 11 where the logarithm of the pressure has been plotted as a function of T_3. The experimental data have been taken from Ref. 1. As can be seen, all results are approximately linear when plotted in this way (i.e., the pressure is an exponential function of T_3). The slopes of TIP4P and TIP4P/2005 models are slightly smaller than the experimental one. TIP4P/Ice model is the best in reproducing the coexistence temperatures for the range of pressures considered in this work. Not only that, but also the slope is in good agreement with experiment. The obvious conclusion of Fig. 11 is that to obtain reliable predictions of T_3 a water model reproducing the experimental melting point of ice I_h is needed. The deviations shown in Fig. 11 can be easily understood when one takes into account that melting point of ice I_h is of 230 K for TIP4P, 250 K for TIP4P/2005, and 270 K for TIP4P/Ice model. The modification of the cross interaction between water-methane employed for the TIP4P/2005 model ($\chi=1.07$) improves the results with respect to the results of this model with $\chi=1$. The TIP4P/2005 model with $\chi=1.07$ predicts values of T_3 that are about 15 K below the experimental values, whereas the deviation is of 20 K when the value $\chi=1$ is used. We have also performed preliminary runs to determine T_3 at 400 bar for TIP4P/2005 water, and the methane-water potential recently proposed by Ashbaugh *et al.*[139] The value obtained of T_3 at 400 bar using this new set of parameters for the methane-water interaction[139] was about 278(8) K, very close to that obtained with TIP4P/2005 and $\chi=1.07$ [281(2) K]. This is not surprising since the water-methane potential in both cases was fitted to reproduce experimental properties of methane in pure water. Regarding Table III, the value of ϵ for the water-methane cross interaction of the TIP4P/Ice ($\chi=1$) and TIP4P/2005 ($\chi=1.07$) models is almost identical: about $\epsilon/k_B=125$ K. That indicates that the methane-water interaction is quite similar for TIP4P/Ice and TIP4P/2005 models with $\chi=1.07$. The difference between the two systems arises not from the water-methane interactions but rather in the water-water interactions which are responsible for the different melting points of the two models.

In a recent paper, Walsh *et al.*[84] performed a study of spontaneous methane hydrate nucleation and growth from computer simulation. In that work, they used an initial configuration of liquid water with methane vapor formed by melting 64 unit cells of sI (2944 water molecules and 512 methane molecules) with a methane mole fraction of 0.15. Notice that the composition used by Walsh *et al.* in their study is that of a system of type *A*. They performed molecular dynamics simulations at 250 K and 500 bar using the TIP4P/Ice model and the same model of CH_4 used here. On the scale of a microsecond they observed the spontaneous nucleation of the methane hydrate. This result is in agreement with the three-phase coexistence line shown in Fig. 11 for this model. Under these conditions the methane hydrate phase is indeed the stable phase. It is interesting to point out that the formation of a bubble was also observed by Walsh *et al.* in their simulations.[84]

A solid can be superheated in *NpT* simulations[140–144] if there is no interface present. However, superheating does not seem to be possible as soon as the solid has an interface,[56] since then the interface acts as a nucleation site. McBride *et al.*[144] determined that in *NpT* simulations ices can be superheated by about 90 K with respect to the equilibrium melting temperature. To determine the stability limit of the methane hydrate we performed *NpT* MD simulations for the solid in the bulk (i.e., without any interface) using the TIP4P/Ice model and fixing the pressure to 100 bar. It was found that at 405 K the system melts rather quickly (in about 0.1 ns), whereas at 395 K the systems did not melt after 30 ns. The evolution of the potential energy as a function of time is shown in Fig. 12. The value of T_3 at 100 bar when using TIP4P/Ice is about 285 K. Therefore, in bulk *NpT* simulations the methane hydrate can be superheated by about 115(5) K with respect to the true equilibrium melting temperature T_3 (the same degree of superheating was found for the other two pressures considered in this work).

IV. CONCLUSIONS

In this work, we have performed molecular dynamics simulations to estimate the three-phase (methane hydrate-water-methane) coexistence temperature T_3 at three different pressures (40, 100, and 400 bar) by using the direct coexist-

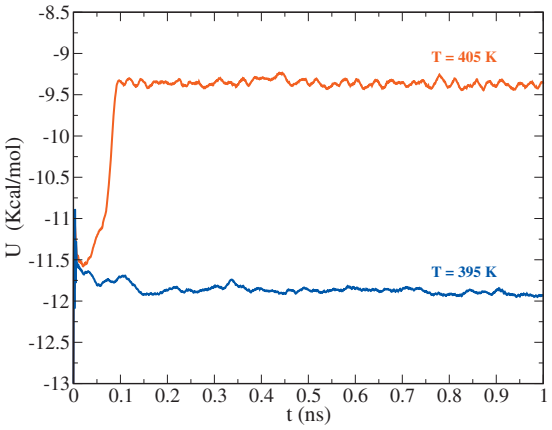

FIG. 12. Evolution of the potential energy as a function of time from *NpT* runs of the methane hydrate in the bulk. Results were obtained at 100 bar using the TIP4P/Ice model for water and a single LJ site for methane. At 405 K (top) the methane hydrate melts quickly on a short time scale (0.1 ns) provoking an increase of the potential energy. At 395 K (bottom) the energy remains constant (with some thermal fluctuations). Even after 30 ns the methane hydrate was stable at this temperature.

ence method. Two systems with different global mole fractions of methane were considered: system *A* which has a methane mole fraction of $x_{CH_4} \sim 0.15$ and system *B* with a methane mole fraction of $x_{CH_4} \sim 0.21$. At temperatures above T_3 the methane hydrate melts for both compositions yielding a two phase (water-methane) system. At temperatures below T_3 the growth of the methane hydrate is observed yielding at the end of the run pure methane hydrate in the case of system *A* and a two phase system (methane hydrate-methane) in the case of system *B*. For systems *A* and *B* the methane hydrate melts layer by layer with the same mechanism. The growth of the methane hydrate takes place slowly and layer by layer in the case of system *B*. In the case of system *A* the growth of the methane hydrate took place quickly after the formation of a supersaturated methane-water solution obtained quickly after the formation of a methane gas bubble in the simulation box. The value obtained for T_3 for systems *A* and *B* was the same (within the statistical uncertainty). Thus, although the kinetic mechanism was different the thermodynamic properties were not affected (as expected). Rather long runs (in 100–1000 ns) are required to determine T_3 accurately. The conclusion is that three-phase direct coexistence simulations can be performed to determine the value of T_3 for the methane-water binary mixture.

Results for T_3 were obtained using three different water models, namely, TIP4P, TIP4P/2005, and TIP4P/Ice with methane described by a simple LJ center. The cross interaction was described by the Lorentz–Berthelot rules. A system with positive deviations from the energetic Lorentz–Berthelot rule (as an effective way of introducing the polarization of methane within the water medium) was also considered for the TIP4P/2005 water model. The results showed that the three-phase coexistence line obtained with the TIP4P/Ice model was in good agreement with the experimental one. Results obtained by TIP4P/2005 and TIP4P models were shifted to lower temperatures by about 20 and 40 K, respectively, with respect to the experimental results. Introducing deviations from Lorentz–Berthelot rule in the case of the TIP4P/2005 model reduces the disagreement with experiment to about 15 K. The deviation found in this work between the T_3 line of the models and that found in experiments correlates quite well with the deviation found between the melting point of ice I_h for these models and the experimental value. Therefore, the message is that to obtain the T_3 line correctly, a model with the correct melting point of ice I_h is required. As a general rule it has been found in this work that the value of T_3 at 400 bar is approximately 28 K above the melting temperature of ice I_h for the considered water model.

Therefore, the combination of TIP4P/Ice model for water and a single LJ center for methane appears as adequate choice for the study of hydrate formation. The second valid option is to combine the TIP4P/2005 model with a single LJ center model for methane but introducing positive deviations from the energetic Lorentz–Berthelot combination rule. Although a shift of T_3 of about 15 K is expected with respect to experiment with this second model, it presents the advantage of accurately describing the chemical potential of methane in water[120] and also of using one of the most reliable water models (TIP4P/2005) for equilibrium[145] and transport properties.[146]

ACKNOWLEDGMENTS

This work has been funded by MICINN (Grant No. FIS2010-16159), by CAM (Project No. P2009/ESP-1691), and by Universidad Complutense de Madrid (Project No. 910570). M.M.C. would like to thank Universidad Complutense de Madrid for the award of a Ph.D. studentship.

[1] E. D. Sloan and C. A. Koh, *Clathrate Hydrates of Natural Gases*, 3rd ed. (CRC, Boca Raton, FL, 2007).
[2] R. K. McMullan and G. A. Jeffrey, J. Chem. Phys. **42**, 2725 (1965).
[3] C. W. Mak and R. K. McMullan, J. Chem. Phys. **42**, 2732 (1965).
[4] J. A. Ripmeester, J. S. Tse, C. I. Ratcliffe, and B. M. Powell, Nature (London) **325**, 135 (1987).
[5] W. C. Child, Q. Rev., Chem. Soc. **18**, 321 (1964).
[6] J. D. Londono, W. F. Kuhs, and J. L. Finney, Nature (London) **332**, 141 (1988).
[7] Y. Koyama, H. Tanaka, and K. Koga, J. Chem. Phys. **122**, 074503 (2005).
[8] M. M. Conde, C. Vega, G. A. Tribello, and B. Slater, J. Chem. Phys. **131**, 034510 (2009).
[9] L. C. Jacobson, W. Hujo, and V. Molinero, J. Phys. Chem. B **113**, 10298 (2009).
[10] V. Molinero and E. B. Moore, J. Phys. Chem. B **113**, 4008 (2009).
[11] G. A. Tribello and B. Slater, J. Chem. Phys. **131**, 024703 (2009).
[12] C. Wei and Z. Hong-Yu, Chin. Phys. Lett. **19**, 609 (2002).
[13] S. W. Rick and D. L. Freeman, J. Chem. Phys. **132**, 054509 (2010).
[14] M. M. Conde, C. Vega, C. McBride, E. G. Noya, R. Ramírez, and L. M. Sesé, J. Chem. Phys. **132**, 114503 (2010).
[15] J. van der Waals and J. Platteeuw, Adv. Chem. Phys. **2**, 1 (1959).
[16] H. Davy, Philos. Trans. R. Soc. London, Ser. B **101**, 1 (1811).
[17] K. A. Udachin, G. D. Enright, C. I. Ratcliffe, and J. A. Ripmeester, J. Am. Chem. Soc. **119**, 11481 (1997).
[18] T. Uchida, T. Ebinuma, J. Kawabata, and H. Narita, J. Cryst. Growth **204**, 348 (1999).
[19] M. M. Mooijer-van den Heuvel, C. J. Peters, and J. de Swaan Arons, Fluid Phase Equilib. **172**, 73 (2000).
[20] S. Takeya, A. Hori, T. Hondoh, and T. Uchida, J. Phys. Chem. B **104**, 4164 (2000).
[21] S. Takeya, T. Ebinuma, T. Uchida, J. Nagao, and H. Narita, J. Cryst. Growth **237–239**, 379 (2002).
[22] D. K. Staykova, W. F. Kuhs, A. N. Salamatin, and T. Hansen, J. Phys. Chem. B **107**, 10299 (2003).

[23] K. C. Hester, Z. Huo, A. L. Ballard, C. A. Koh, K. T. Miller, and E. D. Sloan, J. Phys. Chem. B **111**, 8830 (2007).
[24] L. J. Florusse, C. J. Peters, J. Schoonman, K. C. Hester, C. A. Koh, S. F. Dec, K. N. Marsh, and E. D. Sloan, Science **306**, 469 (2004).
[25] F. Schüth, Nature (London) **434**, 712 (2005).
[26] H. Lee, J. Lee, D. Y. Kim, J. Park, Y. Seo, H. Zeng, I. L. Moudrakovski, C. I. Ratcliffe, and J. A. Ripmeester, Nature (London) **434**, 743 (2005).
[27] T. A. Strobel, C. A. Koh, and E. D. Sloan, J. Phys. Chem. B **112**, 1885 (2008).
[28] T. A. Strobel, E. D. Sloan, and C. A. Koh, J. Chem. Phys. **130**, 014506 (2009).
[29] A. Martín and C. J. Peters, J. Phys. Chem. B **113**, 7558 (2009).
[30] I. Aya, K. Yamane, and N. Yamada, in *Proceedings of the First International Offshore and Polar Engineering Conference*, edited by J. S. Chung, B. J. Natvig, K. Kaneko, and A. J. Ferrante (International Society of Offshore and Polar Engineers, Edinburgh, 1991), p. 427.
[31] J. P. Long and E. D. Sloan, Int. J. Thermophys. **17**, 1 (1996).
[32] H. Herzog, K. Caldeira, and E. Adams, in *Encyclopedia of Ocean Sciences*, edited by J. Steele, S. Thorpe, and K. Turekian (Academic, London, 2001), Vol. 1, p. 408.
[33] E. M. Yezdimer, P. T. Cummings, and A. A. Chialvo, J. Phys. Chem. A **106**, 7982 (2002).
[34] T. Kin, T. Nemoto, K. Makino, and K. Koide, in *First International Conference on Innovative Computing, Information and Control (ICICIC)*, edited by J.-S. Pan, P. Shi, and Y. Zhao (IEEE Computer Society, Beijing, 2006), p. 4.
[35] K. A. Kvenvolden, Chem. Geol. **71**, 41 (1988).
[36] G. J. MacDonald, Annual Review of Energy **15**, 53 (1990).
[37] C. Bourry, J. Charlou, J. Donval, M. Brunelli, C. Focsa, and B. Chazallon, Geophys. Res. Lett. **34**, L22303 (2007).
[38] H. Lu, Y. Seo, J. Lee, I. Moudrakovski, J. A. Ripmeester, N. R. Chapman, R. B. Coffin, G. Gardner, and J. Pohlman, Nature (London) **445**, 303 (2007).
[39] E. D. Sloan, Nature (London) **426**, 353 (2003).
[40] J. P. Henriet and J. Mienert, *Gas Hydrates Relevance to World Margin Stability and Climatic Change* (The Geological Society, London, 1998).
[41] S. Grandum, A. Yabe, K. Nakagomi, M. Tanaka, F. Takemura, Y. Kobayashi, and P. E. Frivik, J. Cryst. Growth **205**, 382 (1999).
[42] J. S. Pic, J. M. Herri, and M. Cournil, Can. J. Chem. Eng. **79**, 374 (2001).
[43] C. A. Koh, R. E. Westacott, W. Zhang, K. Hirachand, J. L. Creek, and A. K. Soper, Fluid Phase Equilib. **194–197**, 143 (2002).
[44] C. Moon, P. C. Taylor, and P. M. Rodger, Can. J. Phys. **81**, 451 (2003).
[45] D. M. Duffy, C. Moon, and P. M. Rodger, Mol. Phys. **102**, 203 (2004).
[46] I. M. Svishchev and P. G. Kusalik, Phys. Rev. Lett. **73**, 975 (1994).
[47] I. R. Craig and D. E. Manolopoulos, J. Chem. Phys. **123**, 034102 (2005).
[48] M. Martin-Conde, C. Vega, and L. G. MacDowell, J. Chem. Phys. **125**, 116101 (2006).
[49] L. Vrbka and P. Jungwirth, J. Mol. Liq. **134**, 64 (2007).
[50] Y. Takii, K. Koga, and H. Tanaka, J. Chem. Phys. **128**, 204501 (2008).
[51] T. E. Markland and D. E. Manolopoulos, J. Chem. Phys. **129**, 024105 (2008).
[52] C. Vega, E. Sanz, J. L. F. Abascal, and E. Noya, J. Phys.: Condens. Matter **20**, 153101 (2008).
[53] E. G. Noya, M. M. Conde, and C. Vega, J. Chem. Phys. **129**, 104704 (2008).
[54] E. G. Noya, C. Vega, L. M. Sesé, and R. Ramírez, J. Chem. Phys. **131**, 124518 (2009).
[55] C. McBride, C. Vega, E. G. Noya, R. Ramírez, and L. M. Sesé, J. Chem. Phys. **131**, 024506 (2009).
[56] C. Vega, M. Martin-Conde, and A. Patrykiejew, Mol. Phys. **104**, 3583 (2006).
[57] P. Ungerer, C. Nieto-Draghi, B. Rousseau, G. Ahunbay, and V. Lachet, J. Mol. Liq. **134**, 71 (2007).
[58] M. M. Conde, C. Vega, and A. Patrykiejew, J. Chem. Phys. **129**, 014702 (2008).
[59] D. Quigley and P. M. Rodger, J. Chem. Phys. **128**, 154518 (2008).
[60] J. L. Aragones, M. M. Conde, E. G. Noya, and C. Vega, Phys. Chem. Chem. Phys. **11**, 543 (2009).
[61] C. Vega, M. M. Conde, C. McBride, J. L. F. Abascal, E. G. Noya, R. Ramírez, and L. M. Sesé, J. Chem. Phys. **132**, 046101 (2010).
[62] J. S. Tse, M. L. Klein, and I. R. McDonald, J. Phys. Chem. **4198**, 87 (1983).
[63] P. M. Rodger, J. Phys. Chem. **93**, 6850 (1989).
[64] P. M. Rodger, J. Phys. Chem. **94**, 6080 (1990).
[65] L. A. Báez and P. Clancy, Ann. N.Y. Acad. Sci. **715**, 177 (1994).
[66] K. R. O. Forrisdahl, B. Kvamme, and A. D. Haymet, Mol. Phys. **89**, 819 (1996).
[67] H. Tanaka, Y. Tamai, and K. Koga, J. Phys. Chem. B **101**, 6560 (1997).
[68] A. A. Chialvo, M. Houssa, and P. T. Cummings, J. Phys. Chem. B **106**, 442 (2002).
[69] C. Moon, P. C. Taylor, and P. M. Rodger, J. Am. Chem. Soc. **125**, 4706 (2003).
[70] N. J. English and J. M. D. MacElroy, J. Comput. Chem. **24**, 1569 (2003).
[71] N. J. English and J. M. D. MacElroy, J. Chem. Phys. **120**, 10247 (2004).
[72] B. J. Anderson, M. Z. Bazanta, J. W. Tester, and B. L. Trout, J. Am. Chem. Soc. **109**, 8153 (2005).
[73] V. Chihaia, S. Adams, and W. F. Kuhs, Chem. Phys. **317**, 208 (2005).
[74] C. Moon, R. W. Hawtin, and P. M. Rodger, Faraday Discuss. **136**, 367 (2007).
[75] G. Guo, Y. Zhang, M. Li, and C. Wu, J. Chem. Phys. **128**, 194504 (2008).
[76] H. Jiang, E. M. Myshakin, K. D. Jordan, and R. P. Warzinski, J. Phys. Chem. B **112**, 10207 (2008).
[77] J. F. Zhang, R. W. Hawtin, Y. Yang, E. Nakagava, M. Rivero, S. K. Choi, and P. M. Rodger, J. Phys. Chem. B **112**, 10608 (2008).
[78] S. K. Reed and R. E. Westacott, Phys. Chem. Chem. Phys. **10**, 4614 (2008).
[79] B. Peters, N. E. R. Zimmermann, G. T. Beckham, J. W. Tester, and B. L. Trout, J. Am. Chem. Soc. **130**, 17342 (2008).
[80] E. A. Mastny, C. A. Miller, and J. J. de Pablo, J. Chem. Phys. **129**, 034701 (2008).
[81] E. M. Myshakin, H. Jiang, R. Warzinski, and K. D. Jordan, J. Phys. Chem. A **113**, 1913 (2009).
[82] N. J. English, J. S. Tse, and D. J. Carey, Phys. Rev. B **80**, 134306 (2009).
[83] M. Matsumoto, Journal of Physical Chemistry Letters **1**, 1552 (2010).
[84] M. R. Walsh, C. A. Koh, E. D. Sloan, A. K. Sum, and D. T. Wu, Science **326**, 1095 (2009).
[85] P. G. Debenedetti and S. Sarupria, Science **326**, 1070 (2009).
[86] J. L. F. Abascal, E. Sanz, R. G. Fernandez, and C. Vega, J. Chem. Phys. **122**, 234511 (2005).
[87] S. J. Goodbody, K. Watanabe, D. MacGowan, J. P. R. B. Walton, and N. Quirke, J. Chem. Soc., Faraday Trans. **87**, 1951 (1991).
[88] G. J. Guo, Y. G. Zhang, Y. J. Zhao, K. Refson, and S. G. H. Shan, J. Chem. Phys. **121**, 1542 (2004).
[89] G. J. Guo, Y. G. Zhang, and H. Liu, J. Phys. Chem. C **111**, 2595 (2007).
[90] S. J. Wierzchowski and P. A. Monson, Ind. Eng. Chem. Res. **45**, 424 (2006).
[91] S. J. Wierzchowski and P. A. Monson, J. Phys. Chem. B **111**, 7274 (2007).
[92] I. Nezbeda, W. R. Smith, and J. Kolafa, J. Chem. Phys. **100**, 2191 (1994).
[93] I. Nezbeda, J. Kolafa, J. Pavlicek, and W. R. Smith, J. Chem. Phys. **102**, 9638 (1995).
[94] R. E. Westacott and P. M. Rodger, Chem. Phys. Lett. **262**, 47 (1996).
[95] W. L. Jorgensen, J. Chandrasekhar, J. D. Madura, R. W. Impey, and M. L. Klein, J. Chem. Phys. **79**, 926 (1983).
[96] J. L. F. Abascal and C. Vega, J. Chem. Phys. **123**, 234505 (2005).
[97] A. J. C. Ladd and L. Woodcock, Chem. Phys. Lett. **51**, 155 (1977).
[98] A. J. C. Ladd and L. Woodcock, Mol. Phys. **36**, 611 (1978).
[99] J. Neil Cape and L. V. Woodcock, Chem. Phys. Lett. **59**, 271 (1978).
[100] R. G. Fernández, J. L. F. Abascal, and C. Vega, J. Chem. Phys. **124**, 144506 (2006).
[101] M. Yousuf, S. B. Qadri, D. L. Knies, K. S. Grabowski, R. B. Coffin, and J. W. Pohlman, Appl. Phys. A: Mater. Sci. Process. **78**, 925 (2004).
[102] L. Pauling, *The Nature of the Chemical Bond and the Structure of Molecules and Crystals; An Introduction to Modern Structural Chemistry* (Cornell University Press, Ithaca, 1960).
[103] F. Hollander and G. A. Jeffrey, J. Chem. Phys. **66**, 4699 (1977).
[104] S. W. Peterson and H. A. Levy, Acta Crystallogr. **1957**, 72 (1957).
[105] V. Buch, P. Sandler, and J. Sadlej, J. Phys. Chem. B **102**, 8641 (1998).
[106] J. D. Bernal and R. H. Fowler, J. Chem. Phys. **1**, 515 (1933).
[107] Z. Huo, K. Hester, E. D. Sloan, and K. T. Miller, AIChE J. **49**, 1300 (2003).
[108] D. Van Der Spoel, E. Lindahl, B. Hess, G. Groenhof, A. E. Mark, and H. J. C. Berendsen, J. Comput. Chem. **26**, 1701 (2005).
[109] S. Nosé, J. Chem. Phys. **81**, 511 (1984).
[110] W. G. Hoover, Phys. Rev. A **31**, 1695 (1985).

[111] M. Parrinello and A. Rahman, J. Appl. Phys. **52**, 7182 (1981).
[112] S. Nosé and M. L. Klein, Mol. Phys. **50**, 1055 (1983).
[113] J. P. Ryckaert, G. Ciccotti, and H. J. C. Berendsen, J. Comput. Phys. **23**, 327 (1977).
[114] H. J. C. Berendsen and W. F. van Gusteren, *Proceedings of the NATO Advanced Study Institute on Molecular Liquids* (Reidel, Dordrecht, 1984), pp. 475–500.
[115] U. Essmann, L. Perera, M. L. Berkowitz, T. Darden, H. Lee, and L. G. Pedersen, J. Chem. Phys. **103**, 8577 (1995).
[116] B. Guillot and Y. Guissani, J. Chem. Phys. **99**, 8075 (1993).
[117] D. Paschek, J. Chem. Phys. **120**, 6674 (2004).
[118] M. G. Martin and J. I. Siepmann, J. Phys. Chem. B **102**, 2569 (1998).
[119] W. L. Jorgensen, J. D. Madura, and C. J. Swenson, J. Am. Chem. Soc. **106**, 6638 (1984).
[120] H. Docherty, A. Galindo, C. Vega, and E. Sanz, J. Chem. Phys. **125**, 074510 (2006).
[121] J. S. Rowlinson and F. L. Swinton, *Liquids and Liquid Mixtures* (Butterworths, London, 1982).
[122] P. J. Dyer, H. Docherty, and P. T. Cummings, J. Chem. Phys. **129**, 024508 (2008).
[123] C. L. Kong, J. Chem. Phys. **59**, 2464 (1973).
[124] J. J. Potoff, J. R. Errington, and A. Z. Panagiotopoulos, Mol. Phys. **97**, 1073 (1999).
[125] G. C. Boulougouris, J. R. Errington, I. G. Economou, A. Z. Panagiotopoulos, and D. N. Theodorou, J. Phys. Chem. B **104**, 4958 (2000).
[126] N. J. English, J. K. Johnson, and C. E. Taylor, J. Chem. Phys. **123**, 244503 (2005).
[127] N. J. English and G. M. Phelan, J. Chem. Phys. **131**, 074704 (2009).
[128] F. Biscay, A. Ghoufi, V. Lachet, and P. Malfreyt, J. Chem. Phys. **131**, 124707 (2009).
[129] C. Vega and E. de Miguel, J. Chem. Phys. **126**, 154707 (2007).
[130] A. Ghoufi, F. Goujon, V. Lachet, and P. Malfreyt, J. Chem. Phys. **128**, 154716 (2008).
[131] L. C. Jacobson and V. Molinero, J. Phys. Chem. B **114**, 7302 (2010).
[132] L. G. MacDowell, V. K. Shen, and J. R. Errington, J. Chem. Phys. **125**, 034705 (2006).
[133] J. Vatamanu and P. G. Kusalik, J. Phys. Chem. B **110**, 15896 (2006).
[134] J. Vatamanu and P. G. Kusalik, J. Chem. Phys. **126**, 124703 (2007).
[135] B. A. Buffett and O. Y. Zatsepina, Mar. Geol. **164**, 69 (2000).
[136] J. Vatamanu and P. G. Kusalik, J. Phys. Chem. B **112**, 2399 (2008).
[137] H. Yu and W. F. van Gunsteren, J. Chem. Phys. **121**, 9549 (2004).
[138] C. Vega, E. Sanz, and J. L. F. Abascal, J. Chem. Phys. **122**, 114507 (2005).
[139] H. S. Ashbaugh, N. J. Collett, H. W. Hatch, and J. A. Staton, J. Chem. Phys. **132**, 124504 (2010).
[140] M. P. Allen and D. J. Tildesley, *Computer Simulation of Liquids* (Oxford University Press, New York, 1987).
[141] G. E. Norman and V. V. Stegailov, Mol. Simul. **30**, 397 (2004).
[142] S.-N. Luo, A. Strachan, and D. C. Swift, J. Chem. Phys. **120**, 11640 (2004).
[143] C. McBride, C. Vega, E. Sanz, and J. L. F. Abascal, J. Chem. Phys. **121**, 11907 (2004).
[144] C. McBride, C. Vega, E. Sanz, L. G. MacDowell, and J. L. F. Abascal, Mol. Phys. **103**, 1 (2005).
[145] C. Vega, J. L. F. Abascal, M. M. Conde, and J. L. Aragones, Faraday Discuss. **141**, 251 (2009).
[146] M. A. González and J. L. F. Abascal, J. Chem. Phys. **132**, 096101 (2010).